

Multiple bosonic mode coupling in the charge dynamics of the electron-doped superconductor $(\text{Pr}_{2-x}\text{Ce}_x)\text{CuO}_4$

E. Schachinger,^{1,*} C. C. Homes,² R. P. S. M. Lobo,³ and J. P. Carbotte^{4,5}

¹*Institute of Theoretical and Computational Physics, Graz University of Technology, A-8010 Graz, Austria*

²*Department of Condensed Matter Physics and Materials Science, Brookhaven National Laboratory, Upton, New York 11973, USA*

³*Laboratoire Photons et Matière (CNRS UPR 5), LPS-ESPCI, Université Pierre et Marie Curie, 10 rue Vauquelin, F-75231 Paris Cedex 5, France*

⁴*Department of Physics and Astronomy, McMaster University, Hamilton, Ontario, Canada N1G 2W1*

⁵*The Canadian Institute for Advanced Research, Toronto, Ontario, Canada M5G 1Z8*

(Received 23 February 2008; revised manuscript received 1 July 2008; published 16 October 2008)

We analyze optical spectroscopy data of the electron-doped superconductor $(\text{Pr}_{2-x}\text{Ce}_x)\text{CuO}_4$ (PCCO) to investigate the coupling of the charge carriers to bosonic modes. The method of analysis is the inversion of the optical scattering rate $\tau_{\text{op}}^{-1}(\omega, T)$ at different temperatures T by means of maximum entropy technique combined with Eliashberg theory. We find that in the superconducting state the charge carriers couple to two dominant modes, one at ~ 12 meV and a second one at ~ 45 meV as well as to a high energy background. The low energy mode shows a strong temperature dependence and disappears at or slightly above the critical temperature T_c . The high energy mode exists above T_c and moves toward higher energies with increasing temperatures. It becomes less prominent at temperatures > 100 K above which it evolves into a typical spin-fluctuation background. In contrast to the hole-doped high- T_c superconductors PCCO proves to be a superconductor close to the dirty limit.

DOI: [10.1103/PhysRevB.78.134522](https://doi.org/10.1103/PhysRevB.78.134522)

PACS number(s): 74.20.Mn, 74.25.Gz, 74.72.-h

I. INTRODUCTION

The optical scattering rate $\tau_{\text{op}}^{-1}(\omega)$ in the infrared regime evolved into an important tool to extract microscopic information on the coupling of charge carriers to bosonic modes in the form of the electron-exchange boson interaction spectral density $I^2\chi(\omega)$ in the high- T_c cuprates. The definition of the optical scattering rate itself is based on a generalized Drude form valid for correlated electron systems,

$$\sigma(\omega, T) = \frac{i\Omega_p^2}{4\pi} \frac{1}{\omega - 2\Sigma_{\text{op}}(\omega, T)}. \quad (1)$$

This equation relates the complex optical self-energy $\Sigma_{\text{op}}(\omega, T)$ at a given temperature T to the complex optical conductivity $\sigma(\omega, T)$. The optical scattering rate is related to the imaginary part of the optical self-energy $\Sigma_{2,\text{op}}(\omega, T)$ via

$$\tau_{\text{op}}^{-1}(\omega, T) = -2\Sigma_{2,\text{op}}(\omega, T) = \frac{\Omega_p^2}{4\pi} \text{Re}\{\sigma^{-1}(\omega, T)\}. \quad (2)$$

Here Ω_p is the plasma frequency and ω an energy variable.

It was first demonstrated by Marsiglio *et al.*¹ that there exists an approximate relation between $I^2\chi(\omega)$ and $\tau_{\text{op}}^{-1}(\omega)$ of the form

$$I^2\chi(\omega) \approx W(\omega) = \frac{1}{2\pi} \frac{d^2}{d\omega^2} \left[\frac{\omega}{\tau_{\text{op}}(\omega)} \right]. \quad (3)$$

This relation is valid only at low temperatures and up to energies at which $W(\omega)$ first becomes negative, i.e., unphysical. This second derivative method was used by Carbotte *et al.*² to demonstrate that in the optimally doped system $\text{YBa}_2\text{Cu}_3\text{O}_{6+\delta}$ (YBCO) the quasiparticles couple to a boson resonance at 41 meV which corresponds to a spin one resonance observed by neutron scattering in the imaginary part of

the spin susceptibility.^{3,4} Moreover, the temperature dependence of this resonance peak was found to be identical to the T variation of the equivalent structure in the spectral function $I^2\chi(\omega)$ derived from optics.⁵ Finally, Schachinger and Carbotte⁶ predicted such a spin one resonance to exist in the thallium compound $\text{Tl}_2\text{Ba}_2\text{CuO}_{6+\delta}$ (Tl2201). This was later confirmed by He *et al.*⁷ using neutron scattering.

The next step in the development of methods, which help us to extract information on the electron-exchange boson interaction spectral density $I^2\chi(\omega)$ from optics, was made by Dordevic *et al.*⁸ who developed a new method based on inverse theory. These authors concentrated on the approximate relation,

$$\tau_{\text{op}}^{-1}(\omega, T) = \tau_{\text{imp}}^{-1} + \int_0^\infty d\nu K(\omega, \nu; T) I^2\chi(\nu), \quad (4)$$

reported by Shulga *et al.*⁹ Equation (4) is based on Eliashberg theory and is valid in the normal state. Here τ_{imp}^{-1} is an energy independent impurity scattering rate and the kernel $K(\omega, \nu; T)$ is given by

$$K(\omega, \nu; T) = \frac{\pi}{\omega} \left[2\omega \coth\left(\frac{\nu}{2T}\right) - (\omega + \nu) \coth\left(\frac{\omega + \nu}{2T}\right) + (\omega - \nu) \coth\left(\frac{\omega - \nu}{2T}\right) \right]. \quad (5)$$

Relation (4) was extended by Carbotte and Schachinger¹⁰ to the superconducting state of a d -wave superconductor at $T = 0$ using the kernel

$$K(\omega, \nu; T=0) = \frac{2\pi}{\omega} \left\langle (\omega - \nu) \theta[\omega - 2\Delta(\vartheta) - \nu] \times E \left(\sqrt{1 - \frac{4\Delta^2(\vartheta)}{(\omega - \nu)^2}} \right) \right\rangle_{\vartheta}. \quad (6)$$

This kernel is based on a clean limit, i.e., $\tau_{\text{imp}}^{-1}=0$, perturbation theory expansion of BCS theory reported by Allen¹¹ for an s -wave superconductor which has also been considered by Dordevic *et al.*⁸ In as much as one can think of a d -wave superconductor as a superposition of s wave with variable gaps, Eq. (6) follows as a first approximate generalization of Allen's work to d wave. Here $\langle \cdots \rangle_{\vartheta}$ denotes the ϑ average which can be limited to the interval $\vartheta \in [0, \pi/4]$ for symmetry reasons. Furthermore, $\Delta(\vartheta) = \Delta \cos(2\vartheta)$ reflecting the d -wave symmetry of the superconducting order parameter. Equation (6) ensures that the optical scattering rate is finite in the superconducting state for $\omega > 0$. Finally, $E(x)$ is the complete elliptic integral of second kind and $\theta(x)$ is the step function.

Equation (6) explains why in the superconducting state of a d -wave superconductor the signatures of the $I^2\chi(\nu)$ spectral density in the optical scattering rate $\tau_{\text{op}}^{-1}(\omega)$ are displaced at least by the gap amplitude Δ .¹²⁻¹⁴ This is in contrast to a classical s -wave superconductor in which those signatures are displaced by $2\Delta_0$, with Δ_0 as the gap edge. Finally, we would like to point out that according to Eq. (4) nonzero contributions to the positive definite spectral density $I^2\chi(\nu)$, i.e., nonzero coupling of charge carriers to an exchange boson at energy ν , will always result in an increase in the optical scattering rate because both kernels, Eqs. (5) and (6), are positive definite. Thus, depressions or pronounced peaks in the optical scattering rate $\tau_{\text{op}}^{-1}(\omega)$ cannot be explained by electron-exchange boson interaction and indicate additional influences such as, for instance, infrared activated phonons or quasiparticle density of states effects.

The spectra derived from the deconvolution of Eq. (4) still contained negative and, thus, unphysical parts. Nevertheless, it was demonstrated by Dordevic *et al.*⁸ that the application of a deterministic constraint can result in the regularization of the problem which allows the removal of unphysical negative values from the inverted spectral function $I^2\chi(\nu)$. The authors also demonstrated that such a regularization can result in a reduced quality of data reproduction.

In a final step, so far, in the development of inversion techniques it was demonstrated by Schachinger *et al.*¹⁵ that the application of maximum entropy techniques¹⁶ maximizing the generalized Shannon-Jaynes entropy,¹⁷

$$S = \sum_{j=1}^N \left[a_j - m_j - a_j \log \frac{a_j}{m_j} \right], \quad (7)$$

to deconvolute Eq. (4) will result in a positive definite spectral density $I^2\chi(\nu)$ ensuring best possible data reproduction. Here, the entropy S measures the distance of a candidate vector $\mathbf{a} = \{a_j | j=1, \dots, N\}$ from the default model vector $\mathbf{m} = \{m_j | j=1, \dots, N\}$ which represents the most probable solution prior to the observation of any data. In case of insufficient background information it should be chosen constant,

i.e., $m_j = \text{const}, \forall j$, as will be done throughout this paper. To compensate for the approximate nature of Eq. (4) an additional least-squares fit procedure based on Eliashberg equations which have been extended to d -wave superconductors (see Appendix) proved, finally, to be very successful in the inversion of optical $\text{Bi}_2\text{Sr}_2\text{CaCu}_2\text{O}_{8+\delta}$ (Bi2212) data at various temperatures and doping levels.¹⁸

All this research resulted in one common denominator: in YBCO, Bi2212, and Tl2201 the optical data suggest coupling of the charge carriers to a pronounced boson mode, an "optical" resonance, at energies which agree in most cases with the energies at which a spin one resonance is found by neutron scattering in the imaginary part of the spin susceptibility. In a new experiment Vignolle *et al.*¹⁹ showed, using neutron scattering, that the imaginary part of the spin susceptibility in optimally doped $(\text{La}_{2-x}\text{Sr}_x)\text{CuO}_4$ (LSCO) develops two peak structures, a resonance at the low energy of 12 meV while the second peak was found at ~ 50 meV. A maximum entropy analysis of optical data reported by Gao *et al.*²⁰ on epitaxial optimally doped LSCO thin films confirmed that, indeed, the electron-boson spectral density $I^2\chi(\omega)$ develops two peaks at the energies reported by neutron scattering.²¹ This is also in agreement with earlier results suggested by Zhou *et al.*²² from angular resolved photoemission spectroscopy (ARPES) experiments in underdoped samples. They interpreted their results as a coupling of the charge carriers to phonons which is in some contrast to the results reported by Vignolle *et al.*¹⁹ and Gao *et al.*²⁰

Neutron scattering experiments by Wilson *et al.*²³ report the existence of a spin one resonance in the imaginary part of the spin susceptibility of $(\text{Pr}_{1-x}\text{LaCe}_x)\text{CuO}_{4-\delta}$ (PLCCO) for $x=0.12$ with its peak at ~ 11 meV. It is centered around $(\pi/2, \pi/2)$ in the two-dimensional CuO Brillouin zone as is the case in all other high- T_c superconductors and it disappears at temperatures above T_c . The doping (x) dependence of this peak was studied by Fujita *et al.*²⁴ Scanning tunneling microscope (STM) experiments performed on the same material by Niestemski *et al.*²⁵ support the existence of such a peak at ~ 10 meV. As optical data are available in the similar system $(\text{Pr}_{2-x}\text{Ce}_x)\text{CuO}_{4-\delta}$ (PCCO) we concentrate in this paper on the task to extract information on the electron-boson spectral density $I^2\chi(\omega)$ from optical scattering rates measured by Homes *et al.*²⁶ on a PCCO single crystal with $x=0.15$ ($T_c=20$ K) and from similar data reported by Zimmers *et al.*^{27,28} on thin epitaxially grown PCCO films with $x=0.15$ ($T_c=21$ K).

In Sec. II we discuss the samples used for the analysis in their main features. Data extraction techniques will also be discussed shortly within this section. Section III concentrates on the analysis of the optical data and the discussion of the important features of the $I^2\chi(\omega)$ spectra derived from optical data. Finally, Sec. IV gives a short summary. An Appendix has been included to provide the necessary background information on the extended d -wave Eliashberg formalism used for impure systems.

II. MATERIALS

A. Optimally doped ($x=0.15$) PCCO single crystal

We concentrate first on the experimental results reported by Homes *et al.*²⁶ for an optimally doped PCCO single crys-

tal ($x=0.15$, $T_c \sim 20$ K). The authors report two plasma frequencies: the first value $\Omega_p = 13\,000 \pm 200$ cm^{-1} (1.64 eV) reflects only those carriers which participate in coherent “Drude” transport and a larger value for $\Omega_p = 19\,300$ cm^{-1} (2.4 eV), which was determined from a modification of the finite-energy f -sum rule.^{29,30} The two values of Ω_p obtained using these different approaches indicate that Ω_p is not well known in this material and that its value depends heavily on the method chosen to extract it from the experiment. This leads to some uncertainty because according to Eq. (2) the plasma frequency sets the scale of the optical scattering rate. The smaller value of Ω_p finds its justification in a two-component system where the Drude response is not directly connected to the midinfrared region which is conceived to be due to another band of electrons; this was the approach used in the original analysis of the PCCO single crystal data.²⁶ However, in this work we use a one-component approach and as a result the larger value of Ω_p is more appropriate. In this view Drude and infrared regions come from the same electrons with the infrared part coming from the incoherent boson-assisted processes, and the Drude originates from the coherent quasiparticle response part of the carrier spectral function. Following this argument, the experimental $\tau_{\text{op}}^{-1}(\omega)$ data have been derived from the raw reflectance data using $\Omega_p = 2.4$ eV together with the dielectric constant at infinity, ϵ_∞ , set equal to 4. It is worth remarking at this point that the dielectric function, $\epsilon(\omega)$, and the conductivity are related through the expression $\sigma(\omega) = -i\omega[\epsilon(\omega) - \epsilon_\infty]/4\pi$. Thus, ϵ_∞ is required to derive the imaginary part of the optical conductivity, and as a consequence the optical scattering rate is also influenced by this important parameter.

The optical scattering rate at the lowest normal state temperature reported (30 K) has a zero frequency offset of ~ 22 meV (~ 177 cm^{-1}) which indicates substantial contributions from impurity scattering. In addition, there are sharp features in the scattering rate shown in Fig. 1(a) at approximately 306, 338, and 434 cm^{-1} (≈ 37.9 , 41.9, and 53.8 meV) which have been identified as the infrared-active E_u lattice vibrations in this material.^{26,31–33} In order to remove this sharp structure from the scattering rate, the dielectric function has been modeled using a series of Lorentz oscillators,

$$\epsilon(\omega)_{\text{osc}} = \sum_j \frac{\omega_{p,j}^2}{\omega_j^2 - \omega^2 - i\gamma_j\omega}, \quad (8)$$

where ω_j , γ_j , and $\omega_{p,j}$ are the frequency, width, and effective plasma frequency of the j th vibration, respectively. The oscillator parameters have been determined from fits to the real part of the optical conductivity using a simple linear background; the fitted oscillator values are then used to generate the phonon contribution to the complex dielectric function which is in turn subtracted from the experimentally determined values for the real and imaginary parts of the dielectric function, allowing the sharp phonon features to be removed from the optical scattering rate, as shown in Fig. 1(b).

B. Optimally doped ($x=0.15$) PCCO thin film

We also analyzed data published on thin films by Zimmer *et al.*^{27,28} and concentrated on the $x=0.15$ sample. The

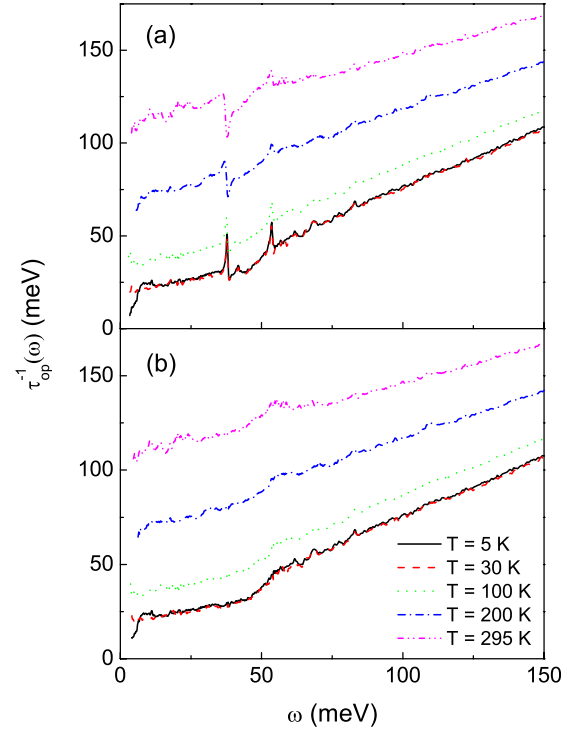


FIG. 1. (Color online) The optical scattering rate $\tau_{\text{op}}^{-1}(\omega)$ in meV in an optimally doped ($x=0.15$) thin PCCO single crystal ($T_c = 20$ K) for several temperatures above and below T_c with (a) the three infrared-active E_u modes at ≈ 306 , 338, and 434 cm^{-1} (≈ 37.9 , 41.9, and 53.8 meV) present and (b) with the same phonons removed.

reflectivity of a thin film also contains information on the optical properties of the underlying substrate. Hence one cannot obtain the film optical functions using a straightforward Kramers-Kronig inversion. In the case of the PCCO films, the substrate response was determined separately. The reflectivity of the total (film plus substrate) system was then fitted by constructing a suitable Drude-Lorentz dielectric function for the film.³⁴ One should note that the parameters used in this Drude-Lorentz dielectric function are not to be taken as representative of intrinsic excitations. They should be looked at as a convenient parametrization of the material dielectric function. Once this dielectric function is known, any other optical function can be generated straightforwardly.

Figure 2(a) presents the optical scattering rate $\tau_{\text{op}}^{-1}(\omega)$ vs ω for the optimally doped epitaxially grown thin PCCO film ($x=0.15$, $T_c = 21$ K). The plasma frequency, calculated from a finite sum rule, is $\Omega_p = 17\,570$ cm^{-1} (2.18 eV) and ϵ_∞ was set to 4. Figure 2(b) shows the scattering rate once phonons have been eliminated.

The zero frequency offset of the optical scattering rate $\tau_{\text{op}}^{-1}(0) = 32.5$ meV (~ 262 cm^{-1}) at $T = 25$ K which suggests a much higher impurity concentration in comparison to the single crystal discussed in Sec. II A. The overall shape of the scattering rate in the $x=0.15$ film is similar to the crystal response. The phonons in the film tend to be broader and less screened by free carriers than in the crystal. These effects are

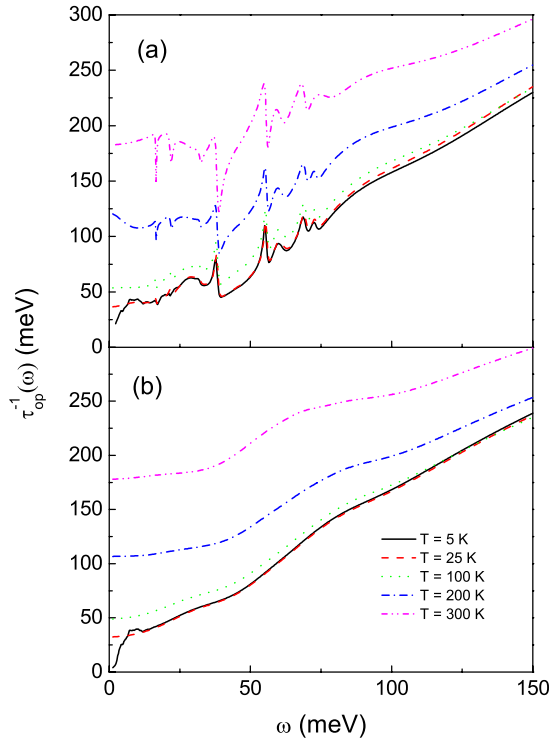


FIG. 2. (Color online) The optical scattering rate $\tau_{\text{op}}^{-1}(\omega)$ in meV in an optimally doped ($x=0.15$) PCCO thin film ($T_c=21$ K) for several temperatures above and below T_c with (a) the infrared-active phonon modes present and (b) with these phonons removed.

consistent with a larger disorder and smaller weight of the coherent peak in the film, as we describe below.

There is a scaling by roughly a factor of 2 required if one wants to compare directly the $x=0.15$ film and crystal data. It comes from the difference in the absolute value of their respective scattering rates. It is worth noticing that this is not an effect originating in the scattering rate of carriers participating in the coherent transport. As discussed in Sec. II A, taking into account the coherent transport alone, the low frequency optical conductivity of the $x=0.15$ single crystal at $T=30$ K can be described by a Drude peak having $\Omega_p=1.61$ eV ($13\,000\text{ cm}^{-1}$) and $\tau_{\text{op}}^{-1}(\omega=0)\approx 11$ meV (90 cm^{-1}). Performing the same analysis on the $x=0.15$ film at $T=25$ K one obtains $\Omega_p=1.18$ eV (9500 cm^{-1}) and $\tau_{\text{op}}^{-1}(\omega=0)=11$ meV. The scattering rate is the same but the weight of the Drude peak in the film is significantly smaller. As the film and the crystal compositions are nominally the same, the f -sum rule states that the area under their respective optical conductivities should be the same. Hence, the weight lost in the coherent peak of the film is redistributed as an incoherent background. This effect will produce, as observed, a higher midinfrared optical conductivity in the film and hence a broader incoherent scattering rate. Thus, a factor of 2 is not far from the difference in dc conductivity [$\sigma_1(\omega)$ extrapolated to $\omega=0$] observed in these two samples ($3 \times 10^4\ \Omega^{-1}\text{ cm}^{-1}$ for the crystal; $1.7 \times 10^4\ \Omega^{-1}\text{ cm}^{-1}$ for the film).

III. DATA ANALYSIS AND DISCUSSION

A. $x=0.15$ PCCO single crystal

Because of the rather large normal state zero frequency offset of the optical scattering rate PCCO can no longer be treated in the clean limit as has been done so far for the systems Bi2212, LSCO, Tl2201, and YBCO. Thus, the impurity scattering rate τ_{imp}^{-1} gains importance in Eq. (4) and has to be treated as an external parameter in the maximum entropy deconvolution of this equation.

The complete inversion procedure consists of two steps. First Eq. (4) together with the appropriate kernel is deconvoluted using a classical maximum entropy method. The default model is set to a constant which is adjusted from temperature to temperature to ensure best possible data reproduction at high energies $\omega > 250$ meV. This results in a first approximation for the electron-exchange boson interaction spectral density $I^2\chi(\omega)$. In a second step this approximate spectral density is refined using a least-squares fit procedure based on the full nonlinear Eliashberg equations [Eq. (A1)]. This second step is of particular importance when inverting superconducting state data.

Figure 3 reports the results of our data analysis. Figure 3(a) demonstrates the quality of data reproduction when the $I^2\chi(\omega)$ spectra shown in Fig. 3(b) are used to calculate the optical scattering rate using the Eliashberg equations [Eq. (A1)]. The heavy lines represent the data and the thin lines the theory. For the normal state, $T=295, 200, 100,$ and 30 K, Eliashberg equation [Eq. (A1b)] with $\tilde{\Delta}(\nu+i0^+; \vartheta) \equiv 0$ was used to calculate the renormalized quasiparticle energies $\tilde{\omega}(\nu+i0^+)$. In this case the impurity scattering rate τ_{imp}^{-1} is only a term which is added to the renormalized energies. An impurity parameter $t^+=3.1$ meV (see Appendix) was required for best over all data reproduction. It corresponds to an impurity scattering rate $\tau_{\text{imp}}^{-1}=2\pi t^+ \approx 19.5$ meV for all temperatures. This is in excellent agreement with the zero frequency offset of ~ 22 meV reported for the $T=30$ K data.

Particular attention is required for the superconducting state. First of all, impurities are always pair breaking in d -wave superconductors and thus effectively reduce the critical temperature of the impure sample in comparison to the “clean limit” critical temperature. Furthermore, there are two limits of impurity scattering to be considered. One limit is described by unitary or resonant scattering which is characterized by the parameter Γ^+ in Eq. (A1b). The other limit is Born’s scattering (or weak scattering) characterized by the impurity parameter t^+ . In reality the scattering law is intermediate between unitary and Born limit scatterings. This is characterized by the parameter c in Eq. (A1b); $c=0$ is the unitary limit and $c \rightarrow \infty$ the Born limit. Another complication arises from the fact that the relevant kernel (6) does not contain impurity scattering in contrast to its normal state counterpart Eq. (5). Furthermore, Eq. (6) requires some knowledge of the size of the gap amplitude Δ . Fortunately, this is not critical in this particular case because the rather big impurity scattering rate of ~ 22 meV suggests that the sample will already be in the gapless regime even at $T=5$ K.³⁵ Thus, it will be sufficient for the first step, the

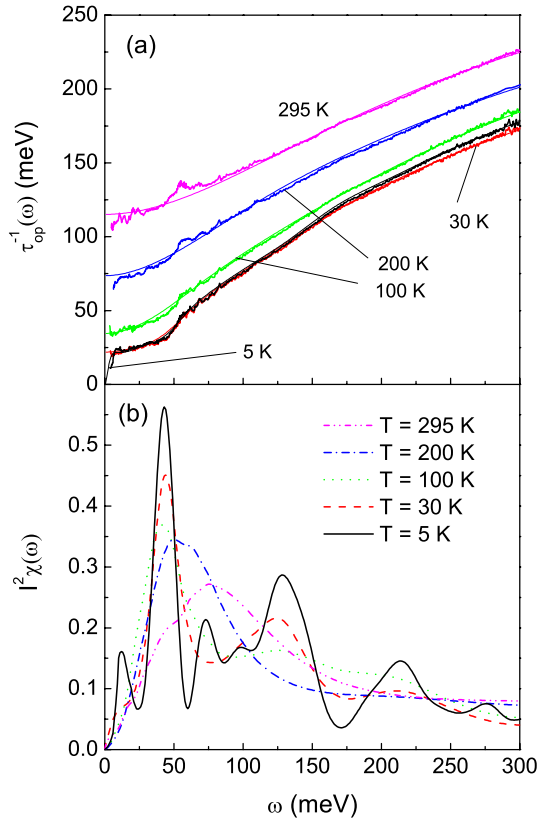


FIG. 3. (Color online) (a) The optical scattering rate $\tau_{op}^{-1}(\omega)$ in meV as a function of ω (in meV) at five temperatures, namely, $T = 300, 200, 100,$ and 30 K in the normal state and $T = 5$ K [the only curve with $\tau_{op}^{-1}(\omega=0) \equiv 0$] in the superconducting state for the optimally doped PCCO single crystal ($x=0.15$). The heavy lines present experimental data, while the light lines correspond to theoretical results obtained from solutions of the full Eliashberg equations [Eq. (A1)] using the $I^2\chi(\omega)$ spectral densities shown in the bottom frame of this figure. The impurity parameter was set to $t^+ = \Gamma^+ = 3.1$ meV. (b) The electron-exchange boson interaction spectral density $I^2\chi(\omega)$ obtained from the inversion of the experimental data presented by the heavy lines in the top frame of this figure.

maximum entropy deconvolution of Eq. (4), to use that value of Δ for which the best data reproduction can be achieved. This procedure results in a first approximation of the $I^2\chi(\omega)$ spectrum which is then parametrized and improved by a least-squares fit to the data using the solutions of the full nonlinear Eliashberg equations to calculate the optical scattering rate. In this step the impurity parameter t^+ stays unchanged and only Born scattering is treated but is included in each iteration of the Eliashberg equations (IV) and, of course, this greatly reduces the value of the critical temperature T_c . The result is the spectral density $I^2\chi(\omega)$ shown by the solid line in Fig. 3(b).

In a final step the low energy regime $0 \leq \omega \leq 10$ meV in which the initial slope of $\tau_{op}^{-1}(\omega)$ is dominated by impurity scattering is to be fitted using full nonlinear Eliashberg theory [Eq. (A1)], taking into account the different laws of impurity scattering. As the scattering rate itself has already been determined, the appropriate scattering law can now be determined by the best possible fit to the data in this low

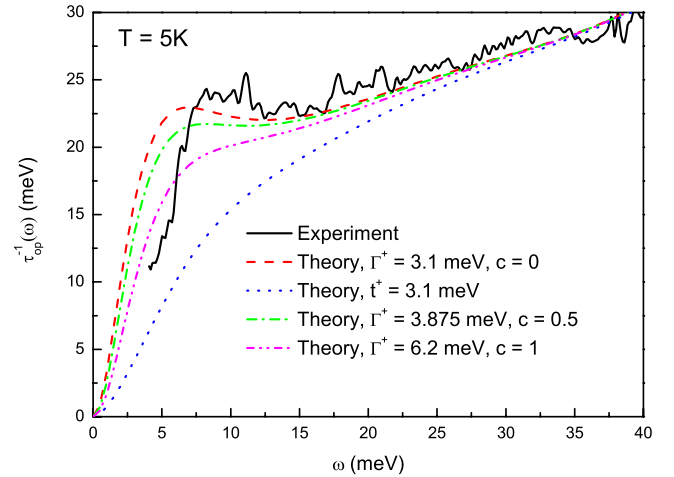


FIG. 4. (Color online) The solid black line represents the experimental $\tau_{op}^{-1}(\omega)$ as a function of ω at $T = 5$ K. The dashed curve presents the results of an Eliashberg theory calculation using unitary impurity scattering described by the impurity parameter $\Gamma^+ = 3.15$ meV. The dotted line corresponds to Born limit scattering described by the parameter $t^+ = 3.15$ meV. Finally, the dashed-dotted curve represents an intermediate case with $\Gamma^+ = 3.94$ meV and $c = 0.5$ and, furthermore, the dashed-double-dotted curve belongs to $\Gamma^+ = 6.3$ meV and $c = 1$.

energy region. Figure 4 demonstrates the results of such a procedure. The solid black line corresponds to the experimental data, the dashed line represents unitary limit scattering with $\Gamma^+ = 3.1$ meV, and the dotted line shows the result for Born limit scattering with $t^+ = 3.1$ meV. For comparison we include additional results for intermediate impurity scattering, namely, $\Gamma^+ = 3.875$ meV and $c = 0.5$ and $\Gamma^+ = 6.2$ meV and $c = 1$. Obviously, impurity scattering is much closer to unitary than to Born-type scattering but it is impossible to decide whether a better fit is found for $c = 0$ (unitary scattering) or $c = 0.5$ (intermediate scattering). It also becomes apparent that impurity scattering does not affect the energy dependence of $\tau_{op}^{-1}(\omega)$ for energies $\omega > 30$ meV and, hence, there is no need to get yet a new estimate for $I^2\chi(\omega)$. It is certainly interesting to note in passing that the clean limit (intrinsic) critical temperature T_{c0} for $t^+ = 0$ is approximately 61 K so that the presence of impurity scattering has greatly reduced the value of the critical temperature.

We return to Fig. 3(b) which presents the spectral densities $I^2\chi(\omega)$ as a result of the inversion process. Five temperatures are shown, namely, $T = 5$ K (solid line), 30 K (dashed line), 100 K (dotted line), 200 K (dashed-dotted line), and 295 K (dashed-double-dotted line). The main feature is a very pronounced peak centered around ~ 45 meV and which gets reduced in amplitude with increasing temperature. This main peak is followed by a valley-hump structure which also becomes less pronounced with increasing temperature and has disappeared at $T = 200$ K. At $T = 295$ K the $I^2\chi(\omega)$ spectral density takes on the simple form proposed by Millis *et al.*³⁶ for a spin-fluctuation spectrum (MMP form) with the maximum at ~ 80 meV. In these respects the $I^2\chi(\omega)$ spectral density found for the optimally doped PCCO single crystal follows the pattern found for all other hole-doped high- T_c superconductors analyzed so far. It is, finally, important to

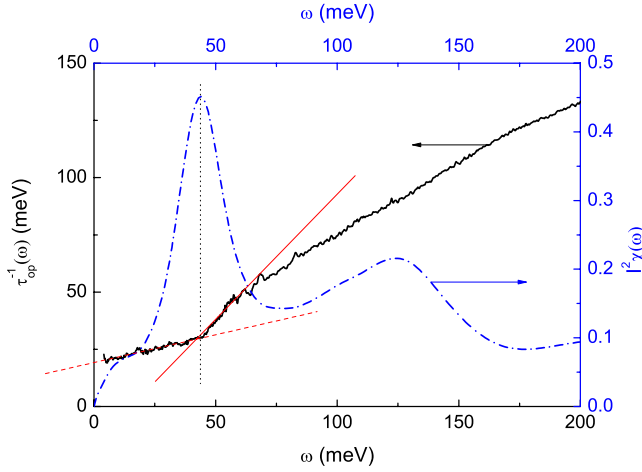


FIG. 5. (Color online) The single crystal experimental optical scattering rate $\tau_{op}^{-1}(\omega)$ as a function of ω at $T=30$ K (black solid line). The two straight lines (red dashed and solid) are used to emphasize the change in slope in $\tau_{op}^{-1}(\omega)$ at $\omega=45$ meV. The (blue) dashed-dotted line corresponds to the spectral density $I^2\chi(\omega)$ derived from the $\tau_{op}^{-1}(\omega)$ data by inversion.

point out that the $T=5$ K shows an additional peak centered around ~ 12.5 meV. This peak describes a possible coupling of the charge carriers to a mode at this energy.

We add Figs. 5 and 6 to make two important points. Figure 5 shows the $\tau_{op}^{-1}(\omega)$ data for $T=30$ K (solid line) for the single crystal. Superimposed are two straight lines. First, the (red) dashed line starts at the $\omega=0$ offset at the value of the residual scattering rate $\tau_{op}^{-1}(\omega=0)$ and follows experiment up to about 45 meV. Second, the (red) solid line starts near the origin and follows the data for energies >45 meV emphasizing the change in slope at $\omega=45$ meV. If the first was perfectly flat (which it is not) the two straight lines would represent two processes, the Drude (coherent) part of the scattering rate and the boson-assisted (incoherent) part. If for the latter we assumed that the boson is an Einstein mode at some energy ω_E which is large enough that the boson-assisted processes are well separated from the coherent Drude part, then the coherent part of $\tau_{op}^{-1}(\omega)$ would be constant and equal to the residual scattering rate at $\omega=0$ until $\omega=\omega_E$ is reached. At ω_E the boson-assisted absorption sets in as an additional process and $\tau_{op}^{-1}(\omega)$ develops a kink as is suggested by the intercept of the two straight lines in Fig. 5. This corresponds precisely to the peak at the same energy seen in the $I^2\chi(\omega)$ spectrum shown as a (blue) dashed-dotted line in Fig. 5 with the horizontal (black) light dotted line indicating the peak center. The kink in $\tau_{op}^{-1}(\omega)$ so identified is a clear signature of the peak at 45 meV in $I^2\chi(\omega)$. Obviously, the (red) dashed straight line has in our case a nonzero slope as a function of energy. This is the signature of additional boson-assisted processes even at energies $\omega < 45$ meV and, consequently, the spectral function $I^2\chi(\omega)$ has nonzero weight at low energies. Next, we will examine this region more closely.

In Fig. 6 we address the question whether or not the low frequency peak at 12.5 meV in the low temperature $I^2\chi(\nu, T=5$ K) spectral density (blue dashed-dotted line) is really essential for data reconstruction in the region $0 \leq \omega$

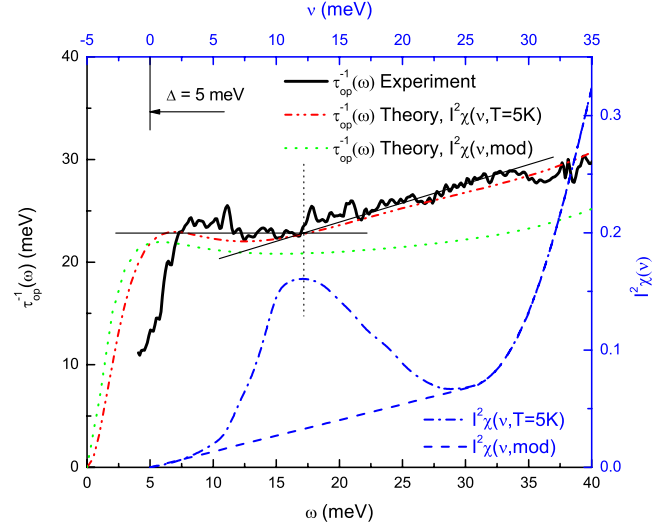


FIG. 6. (Color online) The optical scattering rate $\tau_{op}^{-1}(\omega)$ vs ω for the optimally doped ($x=0.15$) PCCO single crystal in the superconducting state at $T=5$ K. The (black) heavy solid line corresponds to experiment. The two (black) light solid lines are used to emphasize the change in slope in $\tau_{op}^{-1}(\omega)$ at $\omega \approx 17$ meV. The (red) dashed-double-dotted line represents the theoretical $\tau_{op}^{-1}(\omega)$ calculated using the spectral density $I^2\chi(\nu, T=5$ K) (blue dashed-dotted line) for unitary impurity scattering with $\Gamma^+=3.1$ meV and $c=0$. The (green) dotted line shows the theoretical $\tau_{op}^{-1}(\omega)$ calculated using the spectral density $I^2\chi(\nu, mod)$ (blue dashed line) for the same unitary impurity scattering. The ν axis was displaced by the amplitude $\Delta=5$ meV of the superconducting gap at $T=5$ K with respect to the ω axis.

≤ 40 meV and reflects features contained in the $\tau_{op}^{-1}(\omega, T=5$ K) data. The (black) heavy solid line represents the data and, as in Fig. 5, we use two (black) thin straight lines to emphasize the change in slope which takes place at ~ 17 meV in $\tau_{op}^{-1}(\omega, T=5$ K). For comparison we also present the spectral density $I^2\chi(\nu, mod)$ in which the peak around 12.5 meV in spectrum $I^2\chi(\nu, T=5$ K) has been replaced by a straight line connecting the origin with the bottom of the valley at 25 meV (blue dashed line). As required by theory, the ν scale was displaced by the amplitude of the superconducting gap at $T=5$ K, $\Delta=5$ meV. Following the argument already applied in our discussion of Fig. 5 it becomes obvious that the peak at $\nu=12.5$ meV in the spectral density $I^2\chi(\nu, T=5$ K) coincides with the change in slope of the optical scattering rate at ~ 17 meV as indicated by the intersection of the two (black) thin solid lines. Thus, this peak represents, indeed, a real feature of the optical scattering rate and describes the coupling of the charge carriers to a (weak) mode at 12.5 meV.

We added two more curves to this figure. The (red) dashed-double-dotted curve represents the solution of the full nonlinear Eliashberg equations [Eq. (A1)] found for the spectral density $I^2\chi(\nu, T=5$ K) in the superconducting state at $T=5$ K. The impurity parameters were set to $\Gamma^+=3.1$ meV and $c=0$. [It is identical to the (black) thin solid line in Fig. 3(a).] We see that this result follows closely the data over the whole energy region. The second, (green) dotted curve is also for the superconducting state at T

$=5$ K but now the spectral density $I^2\chi(\nu, \text{mod})$ has been used. The impurity parameters remain unchanged. This result falls well below experiment in the region $17 \leq \omega \leq 40$ meV, thus demonstrating the importance of the 12.5 meV peak in $I^2\chi(\nu, T=5$ K) for best possible data reconstruction. It is worth noting that the dashed-double-dotted and the dashed curves meet only at higher energies around 70 meV. This demonstrates clearly that a peak in $I^2\chi(\omega)$ centered around the energy ω_E not only produces a kink in $\tau_{\text{op}}^{-1}(\omega=\omega_E)$ but is also responsible for increased scattering at all energies above ω_E .

B. $x=0.15$ thin PCCO film

We followed the procedure outlined in Sec. III A to invert the optical scattering rate $\tau_{\text{op}}^{-1}(\omega)$ of an optimally doped epitaxially grown thin PCCO film ($x=0.15$, $T_c=21$ K) described in Sec. II B. The best over all data reproduction of the normal state data required an impurity parameter $t^+ = 5.0$ meV which corresponds to an impurity scattering rate $\tau_{\text{imp}}^{-1} = 31.4$ meV (~ 253 cm^{-1}) in excellent agreement with the experimental value of 32.5 meV (~ 262 cm^{-1}) at $T=25$ K. In the superconducting state the best agreement was found for an intermediate impurity scattering strength described by the parameters $\Gamma^+ = 7.8125$ meV and $c=0.75$. We also note that in this case the clean limit critical temperature $T_{c0} \approx 57$ K. This is a remarkable result as it compares well with the intrinsic critical temperature of 61 K found for the single crystal. Thus, we conclude that, indeed, both samples present the same physical properties typical for optimally doped PCCO.

In discussing the results of our data analysis we primarily concentrate on the similarities in the electron-boson spectral densities $I^2\chi(\omega)$ for the two optimally doped samples investigated here. For this purpose Fig. 7 presents the $I^2\chi(\omega)$ spectra for the $x=0.15$ thin film (dashed lines) scaled by a constant factor of 0.5 while the corresponding spectra of the single crystal (solid lines) stay unchanged. Figure 7(a) is for $T=5$ K in the superconducting state and the two spectra reveal very similar features as functions of ω . There is a first resonancelike peak at ~ 14 meV (~ 12 meV in the single crystal) which corresponds in energy to the spin one resonance reported by Wilson *et al.*²³ and to the peak at the same energy found by STM experiments²⁵ in the system PLCCO. There is a second main peak at 50 meV in the thin film sample. The single crystal $I^2\chi(\omega)$ spectrum shows this peak at the slightly lower energy of ~ 45 meV. There exists, as yet, no experimental evidence from neutron scattering for the existence of a corresponding peak in the imaginary part of the spin susceptibility at such an energy in PCCO and, therefore, our analysis represents a specific prediction. This second peak is followed by a valley-hump feature which starts at ~ 80 meV with the hump centered at ~ 107 meV. After this structure the spectral density levels off to a weak background which extends beyond $\omega=300$ meV and which has little structure in the case of the thin film. This result is very similar to what has been reported recently for the system LSCO by analysis of optical data²¹ (including the valley-hump structure) and by neutron scattering.¹⁹ It is interesting

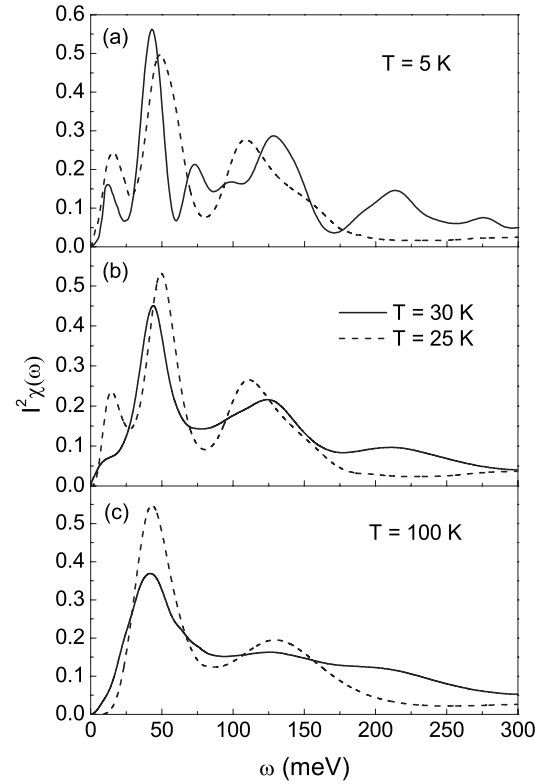


FIG. 7. The electron spectral density $I^2\chi(\omega)$ vs ω for the PCCO $x=0.15$ single crystal (solid lines) and thin film (dashed lines). The $I^2\chi(\omega)$ of the thin film has been scaled by a factor of 0.5 while the single crystal data are unchanged. This emphasizes similarities between the two sets of spectra. The results are (a) for the superconducting state at $T=5$ K, (b) for the normal state at $T=30$ K in the single crystal is compared with the $T=25$ K spectrum for the thin film, and (c) for the normal state at $T=100$ K.

to note an additional valley-peak structure beginning at ~ 55 meV in the single crystal spectrum which cannot be observed at higher temperatures. This structure is most likely due to not completely removed structures in the data around this energy.

Figure 7(b) shows the single crystal results for $T=30$ K (solid line) and the thin film result for $T=25$ K (dashed line) in the normal state, both scaled as described above. While at $T=25$ K a small signature of the 14 meV peak remains, it has basically vanished at $T=30$ K in the single crystal (only a small shoulder is left). These differences could also be due to the very different nature of the two samples. The second peak is still very pronounced and stays basically unchanged in energy in both samples. The valley-hump structure which follows this second peak at around 80 meV stays unchanged in comparison to the $T=5$ K spectra as is the background for $\omega > 200$ meV.

Finally, Fig. 7(c) presents the rescaled spectra for $T=100$ K. We see that all structures have been smeared out in the spectra and the positions of the main peak change only little. The valley-hump structure which follows the main peak has been smeared out almost completely in the $I^2\chi(\omega)$ spectral density of the single crystal while it is still well developed in the thin film spectral density. It is also remarkable that the thin film spectra have a largely suppressed back-

ground for $\omega > 180$ meV in comparison to the single crystal spectra. Increasing the temperature further results in spectra which are MMP-form-like³⁶ and the maximum at $T = 300$ K moves to ~ 80 meV in the thin film and to ~ 90 meV in the single crystal. This corresponds to what has been observed in optimally doped Bi2212.¹⁸

We also note that the maximum of the hump in the $T = 5$ K and 25 K thin film spectra is at lower energies as compared to the same structure in the single crystal spectra. At 100 K, though, they agree that, i.e., in the $x=0.15$ thin film spectra the maximum in the high energy valley-hump structure moves toward higher energies with increasing temperatures while it stays fixed in the single crystal.

IV. SUMMARY

Motivated by the report of a spin one resonance in the imaginary part of the spin susceptibility in the electron-doped system PLCCO at the very low energy of ~ 11 meV by neutron scattering we studied the optical scattering rate reported for optimally doped PCCO samples using the maximum entropy technique to extract information on the electron-boson spectral density $I^2\chi(\omega)$. This spectral density contains information on the coupling of the charge carriers to bosonic modes. We found that in the superconducting state the electrons couple to a bosonic mode centered around 12 (14) meV and that there is a second higher energy group of modes centered around 45 (50) meV which has not yet been observed by neutron scattering. Above T_c the thin film sample still shows some coupling to the low energy mode at 25 K, while in the single crystal no coupling to this mode can be observed at $T=30$ K which can certainly be due to the differences in the two samples. The second high energy peak is clearly developed above T_c in all samples and evolves into an MMP-form-like spin-fluctuation background with further increasing temperature. All $I^2\chi(\omega)$ spectra extend to energies >300 meV. These results resemble very closely to what has been observed in optimally doped LSCO samples and, apart from the low energy mode, what has been reported for optimally doped Bi2212 samples. All this proves that the electron-doped system PCCO behaves in its charge dynamics much like all the other hole-doped high- T_c cuprates. There is one important difference though PCCO, in contrast to all hole-doped high- T_c superconductors investigated so far, is in the dirty limit. The residual scattering in all samples investigated here is sufficiently large to substantially reduce the value of the critical temperature over its pure (intrinsic) limit. This fact is in full agreement with results reported by Dagan *et al.*³⁷ from their analysis of PCCO-lead tunneling junctions.

ACKNOWLEDGMENTS

This research was supported in part by the Natural Sciences and Engineering Research Council of Canada (NSERC) and by the Canadian Institute for Advanced Research (CIFAR). We thank N. Bontemps for valuable discussions and her keen interest. J.P.C. and E.S. want to thank T. Timusk for his interest and many discussions. E.S. enjoyed

the hospitality and friendship of the members of the Department of Physics and Astronomy during his visit at McMaster University. The work at Brookhaven National Laboratory was supported by the Office of Science, U.S. Department of Energy under Contract No. DE-AC02-98CH10886.

APPENDIX: d -WAVE ELIASHBERG EQUATIONS FOR IMPURE SYSTEMS

The generalization to a d -wave gap has already been published by Jiang *et al.*³⁸ and has been used to describe various aspects of the superconducting state in the cuprates. In the mixed representation of Marsiglio *et al.*³⁹ they are of the form

$$\begin{aligned} \tilde{\Delta}(\nu + i0^+; \vartheta) = & \pi T g \sum_{m=0}^{\infty} \cos(2\vartheta) [\lambda(\nu - i\omega_m) \\ & + \lambda(\nu + i\omega_m)] h_{\pm}(i\omega_m) \\ & + i\pi g \int_{-\infty}^{\infty} dz \cos(2\vartheta) I^2 \chi(z) [n(z) \\ & + f(z - \nu)] h_{-}(i\omega_m \rightarrow \nu - z + i0^+), \end{aligned} \quad (\text{A1a})$$

and, in the renormalization channel,

$$\begin{aligned} \tilde{\omega}(\nu + i0^+) = & \nu + i\pi T \sum_{m=0}^{\infty} [\lambda(\nu - i\omega_m) - \lambda(\nu + i\omega_m)] \\ & \times g_{+}(i\omega_m) + i\pi \int_{-\infty}^{\infty} dz I^2 \chi(z) [n(z) + f(z - \nu)] \\ & \times g_{-}(i\omega_m \rightarrow \nu - z + i0^+) + i\pi \Gamma^+ \\ & \times \frac{g_{-}(i\omega_n \rightarrow \nu + i0^+)}{c^2 + g_{-}^2(i\omega_n \rightarrow \nu + i0^+) + h_{-}^2(i\omega_n \rightarrow \nu + i0^+)}. \end{aligned} \quad (\text{A1b})$$

Here,

$$\begin{aligned} h_{\pm}(i\omega_m) = & \left\langle \frac{\tilde{\Delta}(i\omega_m; \vartheta) \cos(2\vartheta)}{\sqrt{\tilde{\omega}^2(i\omega_m) \pm \tilde{\Delta}^2(i\omega_m; \vartheta)}} \right\rangle_{\vartheta}, \\ g_{\pm}(i\omega_m) = & \left\langle \frac{\tilde{\omega}(i\omega_m)}{\sqrt{\tilde{\omega}^2(i\omega_m) \pm \tilde{\Delta}^2(i\omega_m; \vartheta)}} \right\rangle_{\vartheta}, \end{aligned}$$

and the parameter g in Eq. (A1a) allows for a possible difference in spectral density between the $\tilde{\omega}$ and $\tilde{\Delta}$ channels. It is fixed to get the measured value of the critical temperature. In the above $\tilde{\Delta}(i\omega_m; \vartheta)$ is the pairing energy which is evaluated at the fermionic Matsubara frequencies $\omega_m = \pi T(2m - 1)$, $m=0, \pm 1, \pm 2, \dots$, and $\tilde{\omega}(i\omega_m)$ are the renormalized frequencies evaluated at the same Matsubara frequencies; $f(z)$ and $n(z)$ are the Fermi and Bose distributions, respectively. Furthermore, the ϑ dependence of the pairing energy is described by $\tilde{\Delta}(i\omega_m, \vartheta) = \tilde{\Delta}(i\omega_m) \cos(2\vartheta)$ with ϑ as the polar angle in the two-dimensional CuO Brillouin zone. The

brackets $\langle \dots \rangle_{\vartheta}$ are the angular average over ϑ , and $\lambda(\nu) = \int_{-\infty}^{\infty} d\Omega \alpha^2 F(\Omega) / (\nu - \Omega + i0^+)$. Equation (A1) is a set of non-linear coupled equations for the renormalized pairing potential $\tilde{\Delta}(\nu + i0^+; \vartheta)$ and the normalized frequencies $\tilde{\omega}(\nu + i0^+)$ with the gap $\Delta(\nu + i0^+; \vartheta) = \tilde{\Delta}(\nu + i0^+; \vartheta) / Z(\nu)$, where the renormalization function $Z(\nu)$ was introduced in the usual way as $\tilde{\omega}(\nu + i0^+) = \nu Z(\nu)$. Finally, $\tilde{\Delta}(i\omega_n, \vartheta)$ and $\tilde{\omega}(i\omega_n)$ are the solutions of the equivalent equations formulated on the imaginary axis.⁴⁰

Impurity scattering is described by the term proportional to Γ^+ in Eq. (A1b) and enters only this equation because we assume a pure d -wave model for the pairing potential with zero average over the Fermi surface while the impurity scattering is assumed to be isotropic. Here, Γ^+ is proportional to the impurity concentration and c is related to the electron phase shift for scattering off the impurity. For unitary or resonant scattering c is equal to zero while $c \rightarrow \infty$ gives the Born approximation, i.e., the weak scattering limit. In this limit the entire impurity term reduces to the form $i\pi t^+ g(i\omega_n \rightarrow \nu + i0^+)$ with c absorbed into the impurity parameter t^+ . In the normal state $\tilde{\Delta}(\nu + i0^+; \vartheta) \equiv 0$ and there is no need to distinguish any longer between unitary and Born limit impurity scatterings. The scattering term reduces to $i\pi t^+ \text{sgn}[\tilde{\omega}(i\omega_n \rightarrow \nu + i0^+)]$. At the critical temperature linear-

ized Eliashberg equations are valid, i.e., $h(i\omega_n) \simeq 0$ and $g(i\omega_n) \simeq \text{sgn}[\tilde{\omega}(i\omega_n)]$. Thus, at T_c , $t^+ \{c^2 + \text{sgn}[\tilde{\omega}(i\omega_n)]\} = \Gamma^+$ and this relates immediately Γ^+ to the impurity scattering rate via $\tau_{\text{imp}}^{-1} = 2\pi t^+$.

The optical conductivity follows from knowledge of $\tilde{\omega}$ and $\tilde{\Delta}$. The formula to be evaluated is

$$\sigma_{\text{op}}(T, \nu) = \frac{\Omega_D^2 i}{4\pi \nu} \left\langle \int_0^{\infty} d\omega \tanh\left(\frac{\beta\omega}{2}\right) [J(\omega, \nu) - J(-\omega, \nu)] \right\rangle_{\vartheta}. \quad (\text{A2})$$

The function $J(\omega, \nu)$ is given by

$$2J(\omega, \nu) = \frac{1 - N(\omega; \vartheta)N(\omega + \nu; \vartheta) - P(\omega; \vartheta)P(\omega + \nu; \vartheta)}{E(\omega; \vartheta) + E(\omega + \nu; \vartheta)} + \frac{1 + N^*(\omega; \vartheta)N(\omega + \nu; \vartheta) + P^*(\omega; \vartheta)P(\omega + \nu; \vartheta)}{E^*(\omega; \vartheta) - E(\omega + \nu; \vartheta)}, \quad (\text{A3})$$

with $E(\omega; \vartheta) = \sqrt{\tilde{\omega}^2(\omega + i0^+) - \tilde{\Delta}^2(\omega + i0^+; \vartheta)}$, $N(\omega; \vartheta) = \tilde{\omega}(\omega + i0^+) / E(\omega; \vartheta)$, and $P(\omega; \vartheta) = \tilde{\Delta}(\omega + i0^+; \vartheta) / E(\omega; \vartheta)$. Finally, the star refers to the complex conjugate.

*schachinger@itp.tu-graz.ac.at

¹F. Marsiglio, T. Startseva, and J. P. Carbotte, Phys. Lett. A **245**, 172 (1998).
²J. P. Carbotte, E. Schachinger, and D. Basov, Nature (London) **401**, 354 (1999).
³P. Bourges, Y. Sidis, H. F. Fong, B. Keimer, L. P. Regnault, J. Bossy, A. S. Ivanov, D. L. Lilius, and I. Aksay, in *High Temperature Superconductivity*, edited by S. E. Barnes, A. Ashkenazi, J. L. Cohn, and F. Zuo (American Institute of Physics, Woodbury, NY, 1999), p. 207.
⁴P. Dai, H. A. Mook, S. M. Hayden, G. Aeppli, T. G. Perring, R. D. Hunt, and F. Doğan, Science **284**, 1344 (1999).
⁵E. Schachinger, J. P. Carbotte, and D. Basov, Europhys. Lett. **54**, 380 (2001).
⁶E. Schachinger and J. P. Carbotte, Phys. Rev. B **62**, 9054 (2000).
⁷H. He, P. Bourges, Y. Sidis, C. Ulrich, L. Regnault, S. Pailhès, N. S. Berzigiarova, N. N. Kolesnikov, and B. Keimer, Science **295**, 1045 (2002).
⁸S. V. Dordevic, C. C. Homes, J. J. Tu, T. Valla, M. Strongin, P. D. Johnson, G. D. Gu, and D. N. Basov, Phys. Rev. B **71**, 104529 (2005).
⁹S. V. Shulga, O. V. Dolgov, and E. G. Maksimov, Physica C **178**, 266 (1991).
¹⁰J. P. Carbotte and E. Schachinger, Ann. Phys. (Leipzig) **15**, 585 (2006).
¹¹P. B. Allen, Phys. Rev. B **3**, 305 (1971).
¹²A. Abanov, A. V. Chubukov, and J. Schmalian, Phys. Rev. B **63**, 180510(R) (2001).
¹³E. Schachinger and J. P. Carbotte, Phys. Rev. B **64**, 094501 (2001).
¹⁴J. J. Tu, C. C. Homes, G. D. Gu, D. N. Basov, and M. Strongin,

Phys. Rev. B **66**, 144514 (2002).
¹⁵E. Schachinger, D. Neuber, and J. P. Carbotte, Phys. Rev. B **73**, 184507 (2006).
¹⁶E. T. Jaynes, in *Maximum Entropy and Bayesian Methods*, edited by J. Skilling (Kluwer, Dordrecht, 1989).
¹⁷See, for instance, D. S. Sivia, *Data Analysis* (Clarendon, Oxford, 1996), p. 119.
¹⁸J. Hwang, T. Timusk, E. Schachinger, and J. P. Carbotte, Phys. Rev. B **75**, 144508 (2007).
¹⁹B. Vignolle, S. M. Hayden, D. F. McMorrow, H. M. Rønnow, B. Lake, C. D. Frost, and T. G. Perring, Nat. Phys. **3**, 163 (2007).
²⁰F. Gao, D. B. Romero, D. B. Tanner, J. Talvacchio, and M. G. Forrester, Phys. Rev. B **47**, 1036 (1993).
²¹J. Hwang, E. Schachinger, J. P. Carbotte, F. Gao, D. B. Tanner, and T. Timusk, Phys. Rev. Lett. **100**, 137005 (2008).
²²X. J. Zhou *et al.*, Phys. Rev. Lett. **95**, 117001 (2005).
²³S. D. Wilson, P. Dai, S. Li, S. Chi, H. J. Kang, and J. W. Lynn, Nature (London) **442**, 59 (2006).
²⁴M. Fujita, M. Matsuda, S.-H. Lee, M. Nakagawa, and K. Yamada, Phys. Rev. Lett. **101**, 107003 (2008).
²⁵F. C. Niestemski, S. Kunwar, S. Zhou, S. Li, H. Ding, Z. Wang, P. Dai, and V. Madhavan, Nature (London) **450**, 1058 (2007).
²⁶C. C. Homes, R. P. S. M. Lobo, P. Fournier, A. Zimmers, and R. L. Greene, Phys. Rev. B **74**, 214515 (2006).
²⁷A. Zimmers, R. P. S. M. Lobo, N. Bontemps, C. C. Homes, M. C. Barr, Y. Dagan, and R. L. Greene, Phys. Rev. B **70**, 132502 (2004).
²⁸A. Zimmers, J. M. Tomczak, R. P. S. M. Lobo, N. Bontemps, C. P. Hill, M. C. Barr, Y. Dagan, R. L. Greene, A. J. Millis, and C. C. Homes, Europhys. Lett. **70**, 225 (2005).
²⁹D. Y. Smith, in *Handbook of Optical Constants of Solids*, edited

- by E. D. Palik (Academic, New York, 1985), pp. 35–68.
- ³⁰J. Hwang, T. Timusk, A. V. Puchkov, N. L. Wang, G. D. Gu, C. C. Homes, J. J. Tu, and H. Eisaki, *Phys. Rev. B* **69**, 094520 (2004).
- ³¹C. C. Homes, A. W. McConnell, B. P. Clayman, D. A. Bonn, R. Liang, W. N. Hardy, M. Inoue, H. Negishi, P. Fournier, and R. L. Greene, *Phys. Rev. Lett.* **84**, 5391 (2000).
- ³²C. C. Homes, Q. Li, P. Fournier, and R. L. Greene, *Phys. Rev. B* **66**, 144511 (2002).
- ³³M. Braden, L. Pintschovius, T. Uefuji, and K. Yamada, *Phys. Rev. B* **72**, 184517 (2005).
- ³⁴A. F. Santander-Syro, R. P. S. M. Lobo, N. Bontemps, W. Lopera, D. Girata, Z. Konstantinovic, Z. Z. Li, and H. Raffy, *Phys. Rev. B* **70**, 134504 (2004).
- ³⁵A. A. Abrikosov and L. Gor'kov, *Sov. Phys. JETP* **12**, 1243 (1961).
- ³⁶P. Monthoux, A. V. Balatsky, and D. Pines, *Phys. Rev. B* **46**, 14803 (1992).
- ³⁷Y. Dagan, R. Beck, and R. L. Greene, *Phys. Rev. Lett.* **99**, 147004 (2007).
- ³⁸C. Jiang, E. Schachinger, J. P. Carbotte, D. Basov, and T. Timusk, *Phys. Rev. B* **54**, 1264 (1996).
- ³⁹F. Marsiglio, M. Schossmann, and J. P. Carbotte, *Phys. Rev. B* **37**, 4965 (1988).
- ⁴⁰E. Schachinger, J. P. Carbotte, and F. Marsiglio, *Phys. Rev. B* **56**, 2738 (1997).